WELDING RESEARCH

Influence of Ultrasonic Vibration on the Electrophysical Properties of an Arc with a Nonconsumable Electrode

The influence of focused ultrasonic vibration in the arc column with a nonconsumable electrode on the electrophysical characteristics of the arc was explored

BY A. SAVINOV, A. CHUDIN, O. POLESSKY, V. LYSAK, P. KRASIKOV, AND D. MURUGOV

Abstract

In this study, the influence of focused ultrasonic vibration in the arc column with a nonconsumable electrode on the electrophysical characteristics of the arc, near-electrode potential drops, and the shape and structure of the arc column discharge was investigated. It was determined that a focused ultrasonic field in the electrode region of the welding arc leads to an increase in the arc discharge voltage. The impact of a focused ultrasonic field reduces the arc diameter in the anode region and the column. In contrast, near the cathode region, the diameter increases, indicating a change in the nature of the cathodic flow of charged particles in this area.

Keywords

- Nonconsumable Electrode
- Arc
- Ultrasonic Vibration
- Electrophysical Characteristics

Introduction

Gas tungsten arc welding has several advantages over other welding methods. These include process efficiency, versatility, and the ability to produce high-quality welds when fabricating structures for critical applications made of high-alloy and high-strength steel. However, regarding the concentration of thermal energy introduced into the metal, the nonconsumable electrode arc significantly lags behind many well-known welding arc energy sources, resulting in reduced productivity.

Various approaches have been employed to enhance the melting power of nonconsumable electrode arcs, primarily focusing on increasing energy concentration at the heating spot through modulation of the physical parameters of the arc column. Razmyshlyaev et al. (Ref. 1) demonstrated that generating an external electromagnetic field during gas tungsten arc welding effectively enhanced weld quality and overall process efficiency. Rizhov et al. (Ref. 2) proposed that employing a multipolar electromagnetic system allows control of the arc blow, influencing the weld formation process and enhancing arc melting capability. As noted by Boldyrev and Birzhev (Ref. 3), subjecting the arc to a longitudinal magnetic field with a density of up to 0.3 T leads to arc contraction, which increases thermal energy concentration near the heat spot without altering arc heat capacity. This increases the arc hydrodynamic pressure in the melt, reducing the thickness of the liquid thermal insulating layer below the arc. Consequently, penetration depth is increased by a factor of two or more.

Nevertheless, the widespread adoption of the abovementioned method is constrained by the requirement for complex, specialized equipment and the comparative low efficiency in welding ferromagnetic materials under high current conditions. Applying an external magnetic field intensifies erosion of the nonconsumable working area of the electrode (Ref. 4).

Zamkov et al., Tanaka et al., and others (Refs. 5–9) determined that gas tungsten arc welding efficiency can be enhanced by applying activating flux. This flux ensures sufficient arc discharge contraction and greater current

https://doi.org/10.29391/2025.104.012

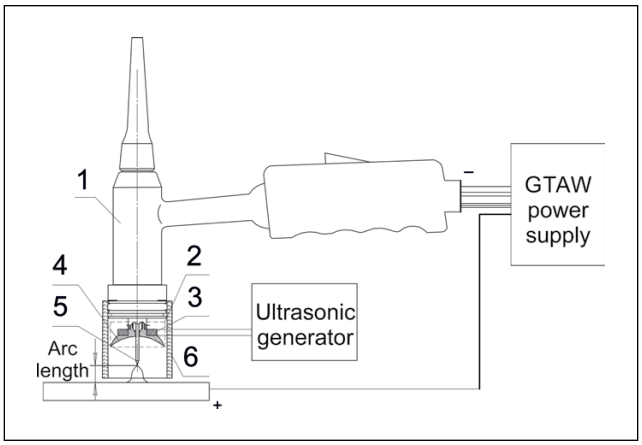

Fig. 1 — Device for welding with a non-consumable electrode under USV: 1 — Welding torch; 2 — piezoelectric transducer; 3 — piezoceramic element; 4 — concave focusing lens; 5 — non-consumable electrode; 6 — protective nozzle.

density in the anode region, increasing the Lorentz force and penetration depth.

Zuber et al. (Ref. 10) proposed that applying SiO_2 flux, which physically constricts the plasma column and reduces the size of the anode spot, tends to increase the energy density of the heat source and the electromagnetic force of the weld pool. This, in turn, results in a threefold increase in penetration depth compared to that achieved through conventional gas tungsten arc welding. According to Ref. 11, arc melting power increases after applying Co_3O_4 and MoO_3 fluxes owing to the reversed Marangoni effect and arc constriction.

However, it should be noted that the flux application has drawbacks, including a negative impact on cathode life and inefficiency for currents exceeding 275 A owing to flux evaporation from the arc without affecting its composition (Ref. 12). Additional drawbacks of flux application include the relatively coarse finish of the weld (Ref. 13) and the requirement for slag removal after welding (Ref. 14).

Fan et al. (Ref. 15) applied a hybrid method of mechanized welding with a consumable electrode in an active gas environment under the influence of ultrasonic waves. They found that ultrasonic waves affect the characteristics of electrode metal transfer and alter the welding arc properties. Under the influence of ultrasonic vibration (USV), the arc contracts, increasing its energy density. A similar method of applying USV to gas tungsten arc welding (U-GTAW) was employed by Wang et al. (Ref. 16). They speculated that using ultrasonic emitting lenses of different diameters increases the intensity of acoustic impact on the arc discharge owing to the increased emission area while maintaining the specified parameters of the piezoelectric transducer. Previous studies have shown that changes in the length and arc diameter column were insignificant when subjected to an acoustic field. In contrast, the arc diameter in the anode region significantly changed due to interference by ultrasonic waves.

According to Wang et al. (Ref. 17), during interaction with ultrasonic waves, the arc is maintained in a stable state without a change in length, but the degree of compression is evident. The maximum compression is observed at emitter heights of 15 and 27 mm (0.591 and 1.063 in.). Xie et al. (Ref. 18) suggested that this is associated with the maximum acoustic pressure formed owing to the resonance of the piezoceramic frequency with the natural frequency of the oscillatory system at the optimal emitter height. The maximum arc compression occurs at a diameter of 31 mm (1.22 in.), indicating the optimal emitter diameter at which the developed acoustic pressure is maximal.

Wu et al. (Ref. 19) applied USV with a frequency of 25 kHz and a power of 500 W to the plasma arc. The oscillations were directly transmitted into the plasma through the electrode, and the chosen high ultrasonic power, determined experimentally, could overcome the compression force of the plasma-forming gas, further compressing the arc. This constriction increased the flow velocity and thermal density within the plasma jet. With an increase in welding current, the degree of arc compression at constant ultrasonic power decreased because the welding current predominantly influenced arc pressure and heating intensity.

Sun et al. (Ref. 20) observed that USV significantly affects the change in force action of the arc. The difference in the peak pressure of the plasma arc on the central axis with and without USV decreased as the current increased from 80 to 120 A. At a welding current of 80 A, the peak force values were 1390 and 1060 Pa with and without ultrasound, respectively, representing a difference of 31%. At a current of 120 A, the maximum arc pressure values were 2098 and 1820 Pa, corresponding to a 15% difference.

Xie et al. (Ref. 21) investigated the quality of weld formation and the depth of melting in arc welding under the influence of acoustic waves on AISI 304 stainless steel plates. They determined that no disruptions in weld formation were observed at all welding modes; however, the depth of melting changed and depended on the ultrasonic emitter height.

Sun et al. (Ref. 22) demonstrated that ultrasonic energy enhances the arc push force, induces continuous high-frequency oscillations in the arc plasma, and increases welding penetration. These effects are believed to contribute to increased welding efficiency and improved aesthetics of stainless steel weld joints.

Thus, the impact of USV leads to a counteraction of the arc discharge and an increase in the concentration of energy introduced into the welding zone. However, the use of stationary devices for gas tungsten arc welding using USV is limited owing to the large size of the piezoelectric transducer and the ineffective cooling of the piezoelements. Another factor complicating the application of such setups is the difficulty in adjusting the oscillation parameters to ensure the necessary conditions for arc–acoustic interaction. These parameters include the distance between the workpiece and the ultrasonic lens, as well as the emission area, which depends on the lens diameter. These issues necessitate designing new device configurations for argon arc welding with the application of USV.

This article presents a device for welding with a nonconsumable electrode focusing the ultrasonic vibrations directly in the welding arc area to provide a stable welding process. Studies were carried out on the influence of focused USV in the column of an arc with a nonconsumable electrode (U-GTAW) on its

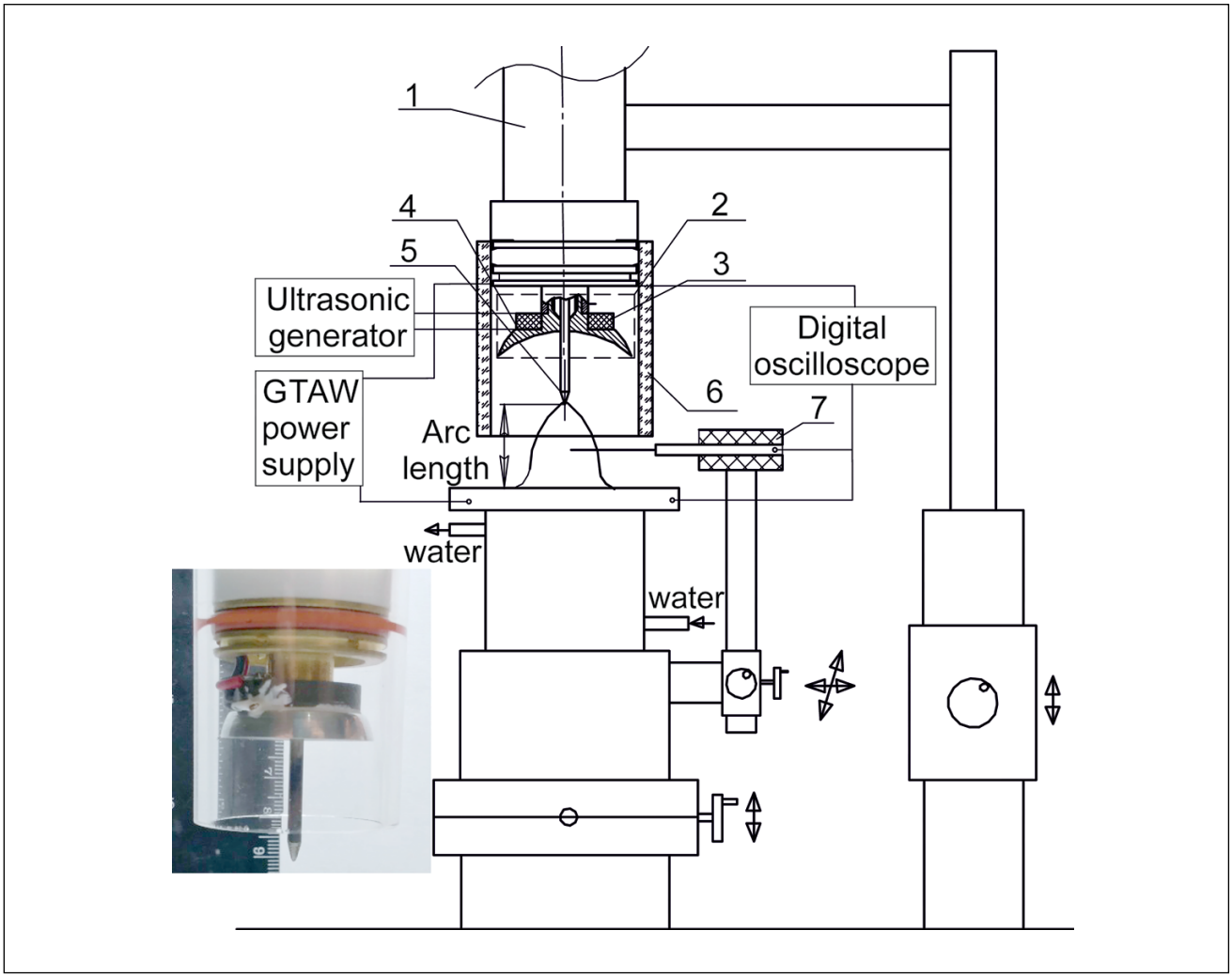

Fig. 2 — Schematic diagram of the setup for probing the welding arc: 1 — Welding torch; 2 — piezoelectric transducer; 3 — piezoelement; 4 — focusing lens; 5 — non-consumable electrode; 6 — protective nozzle; 7 — scanning probe.

electrophysical characteristics, electrode potential drops, and the shape and structure of the arc column discharge.

Experimental Procedure and Setup

Tungsten electrodes with lanthanum oxide additives, WL-20 grade, with diameters ranging from 2.4 to 3.2 mm (0.094 to 0.126 in.) and a tapered working section with an angle α = 30–45 deg and a 0.5-mm (0.02 in.) flat end, were used as nonconsumable electrodes.

The degree of arc counteraction was ensured by the application of high-frequency focused oscillations using a device developed for welding with a nonconsumable electrode under USV (Fig. 1). The PROFARC ATIG 500PAC inverter-type welding machine was used as the power supply for the nonconsumable electrode welding setup.

An arc was initiated to perform the welding process using the power source, and after a certain period (5–10 s), the ultrasonic generator was activated. The voltage at a high frequency (F_{piezo} = 72 kHz) was applied to the piezoelement, which was firmly attached to the concave focusing lens. This application of voltage induced mechanical oscillations in the piezoelement through the action of the electric field (reverse piezoelectric effect), causing the lens to deform at the same frequency, transforming mechanical oscillations into acoustic ones. The lens, with a curvature radius and focal distance equal to 20 mm (0.787 in.), allowed USV to be focused in the welding arc region. The torch design allowed up-and-down nozzle movement with the electrode stickout, providing identical experimental conditions. The rigid attachment of the piezoelectric transducer to the welding torch body prevented overheating of the piezoelectric element, ensuring a stable welding process and prolonged device operation.

The measured length of the standing wave without arc agitation amounted to 4–5 mm. The direct measurement of wavelength in the arc plasma involved considerable difficulties. It is known that the speed of sound is proportional to the square root of absolute temperature. Thus, for a room temperature of 25°C and a plasma temperature of 20,000 K, there will be

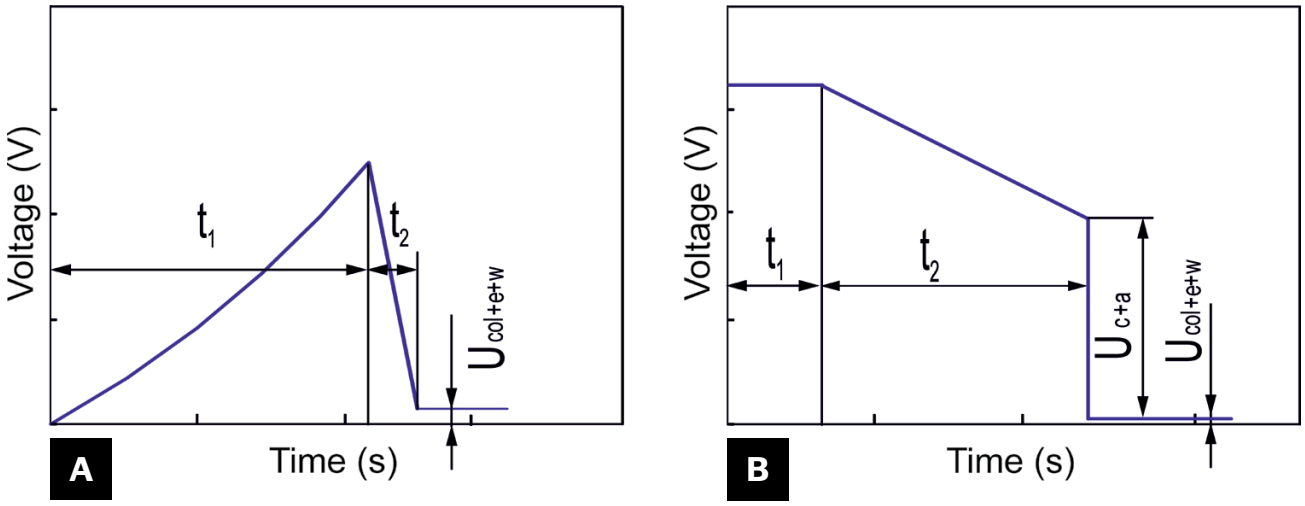

Fig. 3 — Diagram for determining the voltage drop: A — In the cathodic region; B — in the near-electrode regions.

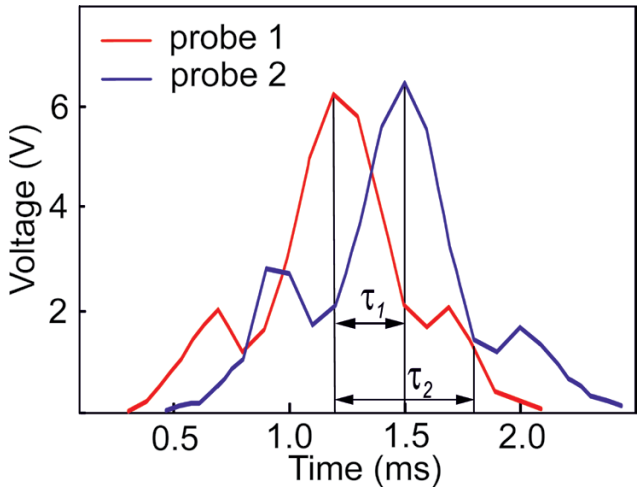

Fig. 4 — Diagram for determining the time intervals τ_1 and τ_2.

a factor of ~ 8 in both wavelengths, resulting in 33–41 mm in the hot part. Of course, the relationship cannot be accurate when there is ionization, but it is a reasonable estimate.

Arc discharge electrophysical properties are commonly studied by methods using a probe — a thin wire made mostly of tungsten — inserted in the arc with measurement of its potential relative to any of the electrodes of discharge. These methods, widely applied in plasma physics, are considered to not allow for high-accuracy measurements for a welding arc study due to the high density of free charges (Refs. 23, 24). In this case, electrons with higher velocity pass faster through the gas layer, which separates the comparatively cold probe and plasma and impacts them with a negative charge. Therefore, the amount of this charge and the probe potential depends on the gas layer thickness, charge concentration, and other factors that the current research techniques cannot consider. The accuracy of the probe methods measurements can be improved by using probes fixed in the arc (Ref. 25) and by using double and triple probes (Ref. 26).

Many arc discharge probing methods use the probes crossing the arc, rotating or moving translationally (Refs. 26–28), stipulated by the necessity to limit the duration of the probe's stay in the arc plasma to prevent its melting. However, optimizing the probing wire diameter and duration of its stay in the arc column significantly reduces the error, making this method applicable. When the fixed probe is used (Ref. 25), it heats in the arc plasma to high temperature, which reduces the negative volume charge near its surface and, therefore, the measurement error.

When using two or more rotating probes passing simultaneously through the arc, the voltage is measured directly between them. In this case, the probe's negative potentials caused by the plasma electrons diffusion are subtracted, and the measurement error is reduced, but the data processing becomes significantly more complicated (Ref. 24).

The data obtained with the probing methods cannot be considered precise as any of these measurement methods cannot precisely account for the probe's disturbance effect on the processes in the arc gap. Nonetheless, considering the good reproducibility of experimental results, such measurements can be considered reliable from a qualitative evaluation viewpoint.

In this study, a single-probe transverse probing method was employed. For this purpose, a laboratory setup was created, the schematic of which is presented in Fig. 2. The piezoelectric transducer, 2, with the firmly attached nonconsumable electrode, 5, was rigidly connected to the holder. An electrically insulated probe, 7, made of tungsten wire with a diameter of 0.25 mm (0.0098 in.), mounted on a stand, was positioned so that the distance between it and the cathode was 1.0 mm (0.039 in.). The length of the arc gap was 4 mm (0.157 in.). After initiating the welding arc, the spring-loaded probe traversed through the arc discharge, and the potential drop value was recorded using an electronic data logger, LA-50 USB. Arc scanning was performed at distances of 1, 2, and 3 mm (0.039, 0.079, and 0.118 in.) from the electrode with and without USV.

The welding current magnitude was 50 A, and the ultrasonic frequency (*f*) was 72 kHz.

The potential drop in the cathodic region was recorded by short-circuiting the scanning probe to the electrode. To achieve this, the probe was brought close to the working section of the nonconsumable electrode, the arc was initiated, and the recorder was activated. As the horizontally moving probe approached the electrode, it entered the peripheral zone of the arc, and at this moment, the potential drop was recorded (Fig. 3A, time t_1). When the electrode contacted the probe, the voltage abruptly dropped (Fig. 3A, t_2), and the difference between the voltage at the moment preceding contact and the newly formed potential reflected the cathodic voltage drop (U_c). The voltage between the line of the newly formed potential and the zero line corresponded to the sum of voltage drops across the clamp, electrode protrusion, and current-carrying wires ($U_{col+e+w}$).

The sum of the cathodic and anodic potential drops was recorded by short-circuiting the electrode to a copper plate to determine the voltage near the anode. As the electrodes (cathode and anode) approached each other, the voltage across the arc gap linearly decreased to a certain value (Fig. 3B, time t_2). Subsequently, the arc discharge was extinguished, and a short circuit occurred with a sudden voltage drop to a value close to zero. The magnitude of the voltage drop before the abrupt jump represented the sum of the cathodic and anodic potentials (Fig. 3B).

The magnitude of the voltage drop in the anodic region is given by:

$$U_a = U_{c+a} - (U_c + U_{col+e+w}) \quad (1)$$

where U_{c+a} is the sum of potential drops in the cathodic and anodic regions, U_c is the voltage drop in the cathodic region, and $U_{col+e+w}$ is the voltage drop across the clamp, electrode, and current-carrying wire.

Video recording was performed simultaneously using two cameras, VS-FAST and Sony NEX-5. An optical filter system was used. Synchronization of the current pulses and frames per second was achieved using an optical trigger of the video camera, and the exposure time was selected from 1/4000 to 1/10000 s.

A method involving transverse probing of the arc with a double horizontal probe was employed to determine the shape and size of the arc discharge with and without USV. The essence of the method is described as follows:

Two probes were rigidly fixed in the probe holder in the horizontal plane at a distance *r* from each other, with the ability to rotate around a vertical axis. The potential of both probes relative to the electrode, as they passed through the arc, was simultaneously recorded using the LA-50 USB recorder. The oscillograms of the probing process are shown in Fig. 4.

The difference between the moments when the probes passed through the axis of the current-carrying channel of the arc column was equal to τ_1 (Fig. 4). Knowing the distance *r* between the probes and the time τ_2 it takes for the current-carrying channel to be traversed by one probe, the diameter of the cross-section of the arc column could be calculated:

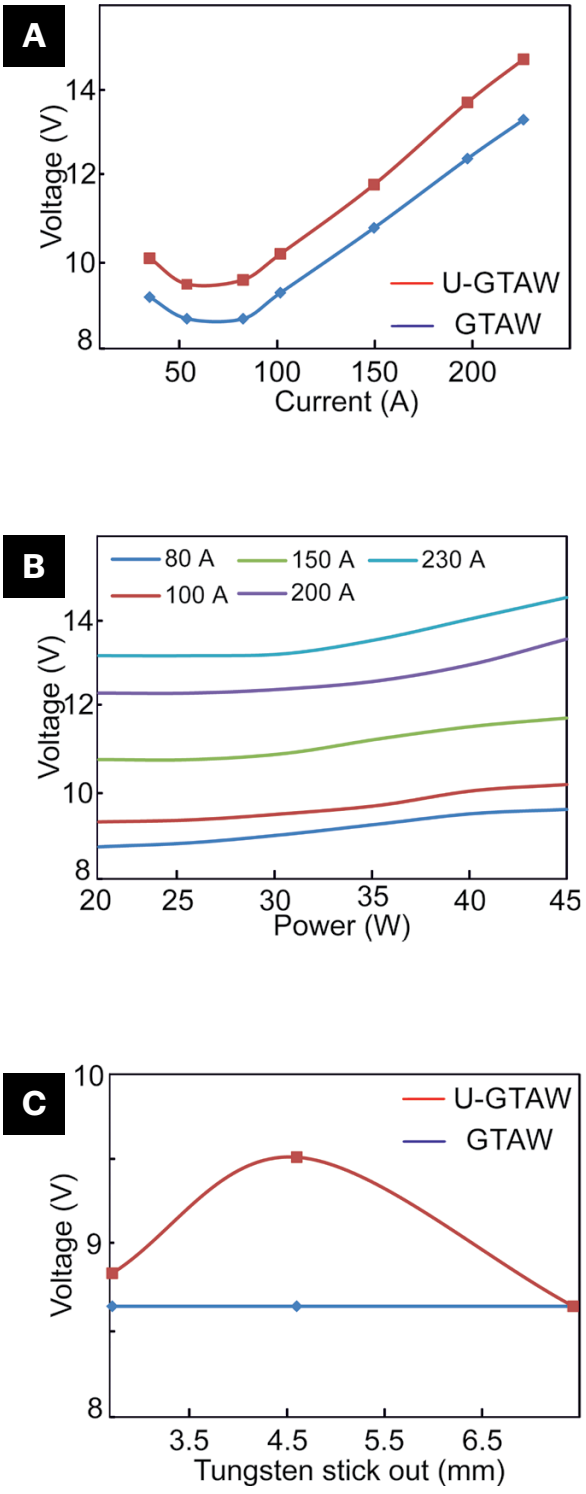

Fig. 5 — A — Arc volt-ampere characteristics; B — dependence of the arc voltage on the ultrasonic power; C — dependence of the arc voltage on the position of focused USV at an arc current of 80 A (at a piezoelectric transducer frequency of 72 kHz, ultrasonic oscillation power of 45 W, nonconsumable electrode diameter of 2.4 mm [0.094 in.], and arc length of 3 mm [0.118 in.]).

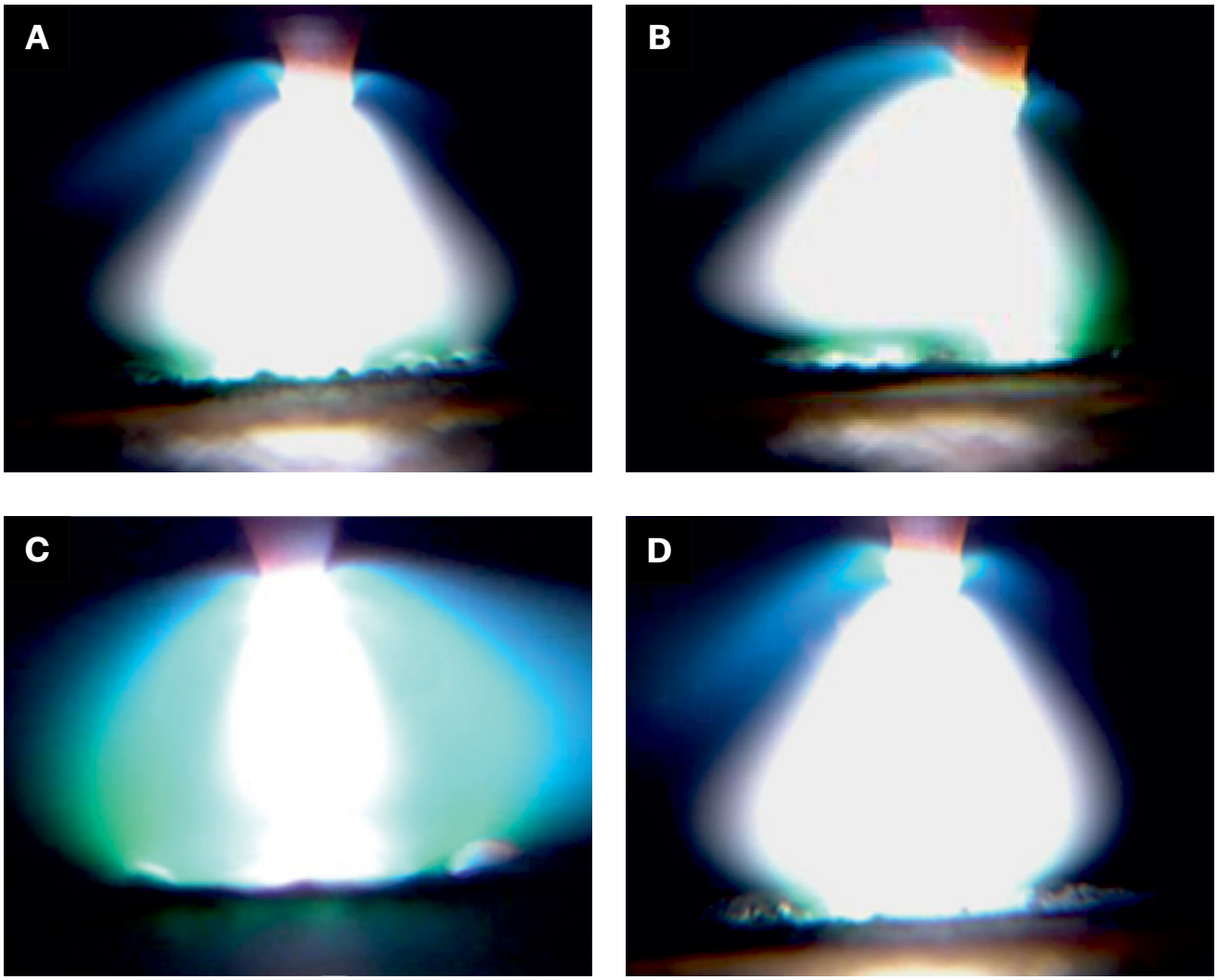

Fig. 6 — Shape of the arc column: A — Without USV; B — USV on the electrode; C — USV in the arc column; D — USV in the welding pool.

$$d_c = \frac{r \cdot \tau_2}{\tau_1} \quad (2)$$

Results and Discussion

Influence of USV on the Static Characteristics of the Arc

A concave focusing lens on the welding torch can lead to turbulence of the shielding gas flow, and a series of experiments were carried out. The penetrations of a plate of AISI 304 steel were carried out both with and without USV. The results showed that in both cases, there was good protection of the weld pool, high-quality formation of penetrations, and the absence of pores. Thus, it can be concluded that the presence of a concave focusing lens and USV did not worsen the quality of gas protection in the case of the torch nozzle diameter, shielding gas flow rate, and distance to the anode used in the experiments.

The static volt-ampere characteristics revealed that the arc with USV existed at a considerably higher voltage compared to that without it (Fig. 5A). The selected range of arc current (30–230 A) with a constant electrode diameter determined the volt-ampere characteristic of the arc, showing the dependence between the established values of current and arc voltage with and without USV in all regions (falling, stable, and rising V–A characteristics).

For an arc length of $l_a = 3$ mm (0.118 in.), the voltage U_{arc} without external factors at a current of 30 A was 9.1 V. Focused USV in the interelectrode gap (arc column) led to an increase in voltage to 10 V under the same welding conditions. As the current increased to 100 A, the voltage difference between the arc with and without USV remained almost unchanged at 0.9 V. A further increase in current to 230 A increased the voltage difference to 1.2 V. Presumably, this occurred due to the higher collision rate of charged particles, particularly electrons, in the current-carrying channel of the arc. Under the

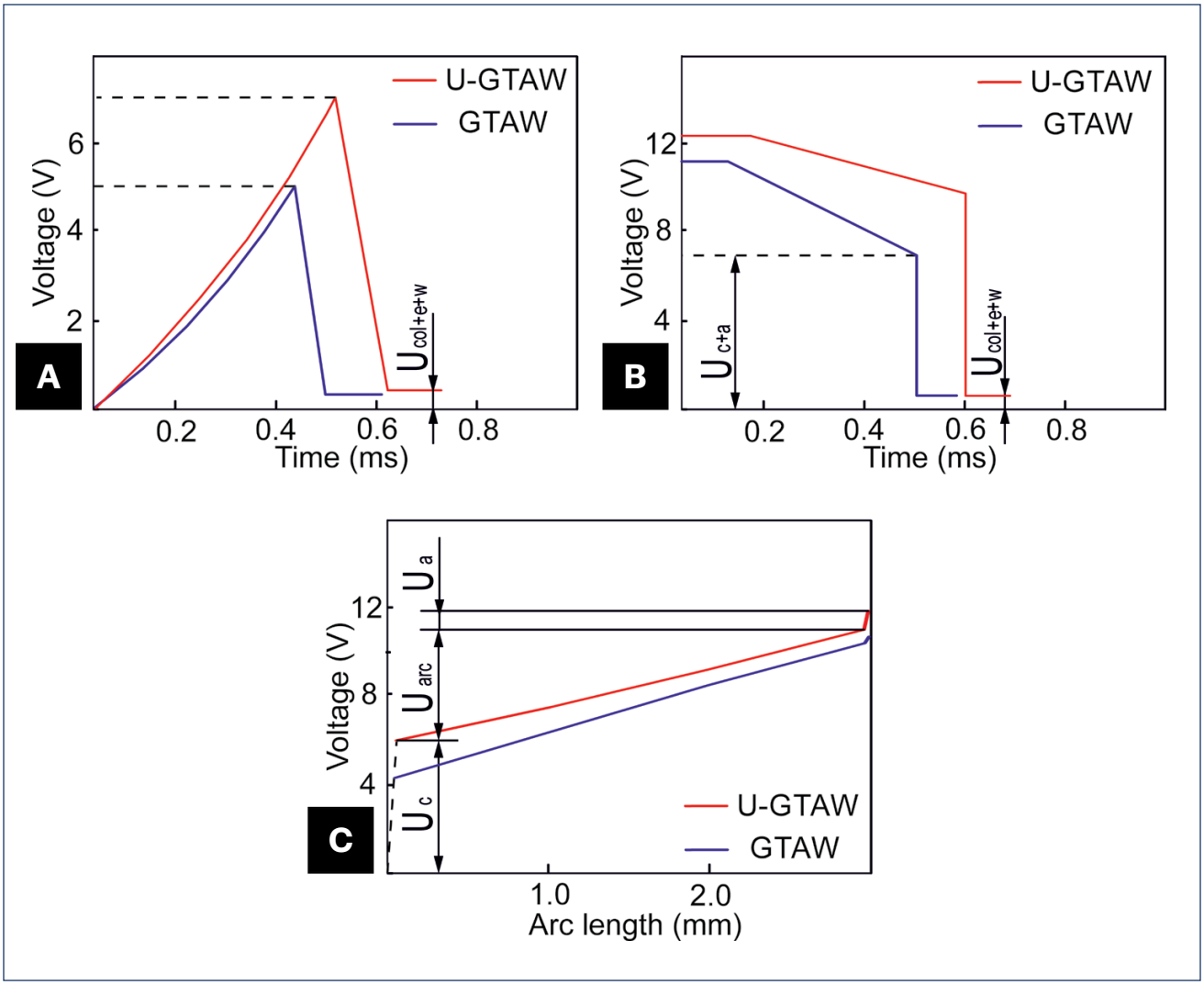

Fig. 7 — Influence of USV: A — On the cathodic potential drop U_c; B — on the possible drop in the near-electrode regions; C — influence of USV and arc length on its voltage drop: U_c — voltage drop in the cathode region, U_{arc} — voltage drop in the arc column, U_a — voltage drop in the anode region.

influence of high-frequency oscillations, these particles more intensively transfered energy, increasing heat generation in the anode region.

With an increase in arc length to 4 mm, its voltage slightly increased (9.7 V at 30 A and 14 V at 230 A). However, the influence of USV diminished, and the voltage difference became 0.8 V, reaching 1.0 V at the maximum current. At an arc length of 5 mm (0.197 in.), U_{arc} was 10.3 and 14.8 V, with a voltage difference increase of 0.7 and 0.8 V at 30 and 230 A, respectively. The reduction in the voltage difference increased under the influence of USV on the arc due to the growth of the arc discharge length and, thus, its volume. Focused USV, having a focal area with a diameter of 2–2.5 mm (0.079–0.098 in.) and constant intensity, could not affect the entire volume of charged particles in the arc, thereby reducing their influence. However, by increasing the intensity of USV, it was possible to compensate for the limited volume of the focal area of USV in the arc column and increase its voltage.

The studies on the influence of ultrasonic power on arc voltage have shown that at low current values (80 and 100 A) (Fig. 5B), the arc, lacking significant rigidity, slightly increases its voltage at low ultrasonic power (~ 13 W). Linear growth of U_{arc} occurs with an increase in ultrasonic power to 23 W, and further power increases practically do not affect the growth of the arc discharge voltage.

Focused low-power USV in the arc column cannot overcome the inherent electromagnetic forces of the arc discharge at high current values (150–230 A) to alter the charged particles' motion characteristics. However, increasing the ultrasonic power to a certain level (above 13 W) increases the arc voltage. In the case of a low-amperage arc, an increase in ultrasonic power does not lead to a significant increase in its voltage. In contrast, in the case of a higher current arc (above 150 A), the growth of U_{arc} becomes linear at the maximum ultrasonic power (Fig. 5B).

Studies on the nature of the impact of focused USV on the electrophysical properties of the arc discharge in different

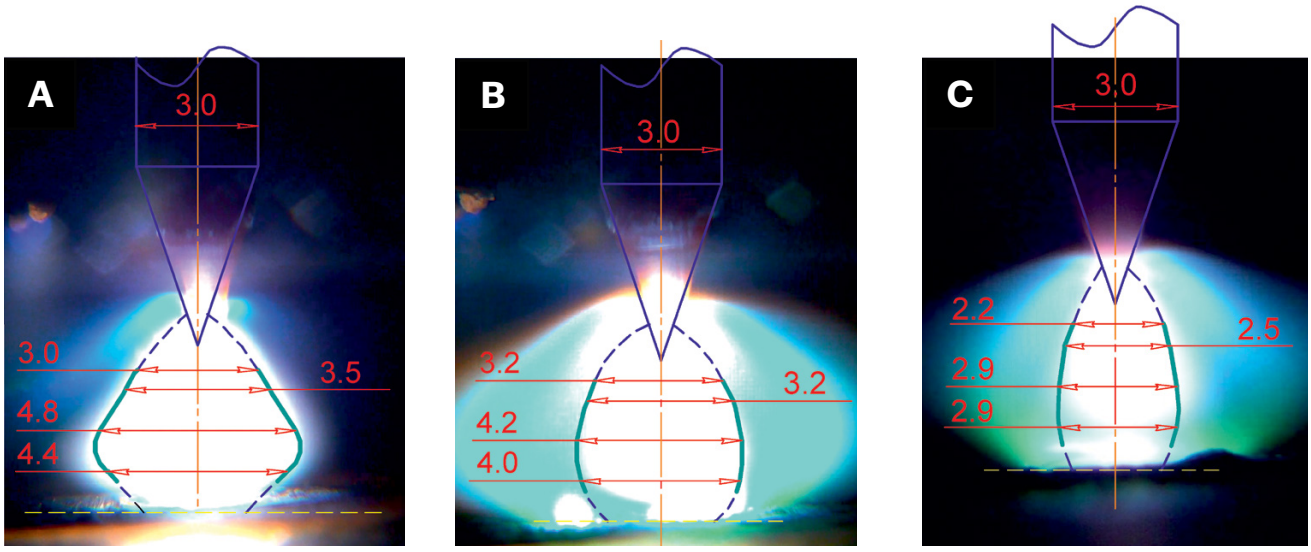

Fig. 8 — Shape of the arc column: A — Without USV (arc current 230 A); B — with USV (arc current 230 A); C — with USV (arc current 150 A).

zones of the welding area (nonconsumable electrode, arc column, and welding pool) showed that positioning the focal area of the USV on the nonconsumable electrode (corresponding to the electrode protrusion of 7.5 mm [0.295 in.] (Fig. 5C) does not increase the arc voltage. In contrast, an unstable discharge position was observed during welding (Fig. 6B). Increasing the arc length did not stabilize its position or increase the voltage. This occurred owing to high-frequency oscillations that hindered the emission of electrons from the cathode, causing the cathode spot to seek a stable position on the electrode where the arc-burning process was stable. As a result, the arc constantly changed its position. When the USV was turned off, the arc stabilized, taking on a classical bell-shaped form (Fig. 6A).

The position of focused USV in the arc column, corresponding to the electrode protrusion of 4.5 mm (0.177 in.) (Fig. 5C), contributed to a sudden increase in voltage. It also lead to the contraction of the arc discharge (Fig. 6C) with a stable position during welding. Initially, the arc tended to diametrically decrease near the anode spot, accompanied by an increase in brightness in this area and, presumably, an increase in heat dissipation in the welded part. At the same time, the arc column near the cathode slightly increased in diameter and occupied a larger area on the electrode than during welding without USV. Over time, the arc assumed a uniform cylindrical shape (Fig. 6C) with a smaller column diameter than the arc without USV. Increasing the arc length slightly reduced the difference in the voltage growth of the arc discharge to 0.7–0.8 V while the welding process remained stable, and the arc did not increase in diameter. The presence of the focal area of USV in the welding pool resulted in a small increase in arc voltage (~ 0.1–0.2 V) (Fig. 5C). This occurred because the oscillations generated by the concave-convex focusing lens were directed radially to the focal area. Then, these oscillations were of low intensity and passed through the arc column, causing charged particles to transfer more energy and ultimately leading to a slight increase in arc voltage. In this case, the arc diameter practically did not decrease (Fig. 6D). Increasing the arc length reduced the impact of USV to zero.

Influence of USV on Near-Electrode Voltage Drops

The nature of the change in cathodic potential drop (U_c) with a constant arc current was significantly influenced by focused USV (Fig. 7A). The value of U_c without USV was 5 V, while that with USV at the same current values (50 A) was substantially higher (7 V). As the current strength increased, the cathodic potential dropped without ultrasonic influence initially decreased and then increases when the arc current strength exceeded 100 A. In the case of USV influence on the arc, the value of U_c was higher by 2 V almost throughout the entire current range compared to the cathodic potential drop without USV. At currents close to critical values, the difference slightly decreased and was approximately 1.8–1.9 V. This occurred owing to the increased rigidity of the arc discharge at $I_{arc} > 200$ A when the intensity of USV was not sufficient to overcome the arc's electromagnetic forces and change the electron emission characteristics from the cathode region.

Because it is difficult to measure the anodic potential drop using the transverse scanning method of the arc discharge with a probe, the potential drop measurements in the near-electrode regions of the arc were performed by short-circuiting the cathode to the anode (Fig. 7B). The calculation of the anodic potential drop was performed using Equation 1.

Research has shown that in the case of an arc discharge with USV, the value of U_a is higher by approximately 0.8–1.0 V compared to the value of the arc's anodic potential without USV. Moreover, the increase in current strength does not lead to a significant change in this difference, indicating that heat generation in the anodic region is greater with USV across the entire welding current range.

Fig. 7C shows the distribution of the potential increase in various areas of the arc with and without USV. The main increase in potential occurred in the electrode regions of the discharge, while the potential gradient in the arc column decreased slightly.

Our findings on the potential drop value being higher in the cathodic region than in the anodic one agreed with the other researchers' data. According to Finkelnburg and Maecker (Ref. 23), the anodic potential drop for argon arc welding with tungsten cathode lies between 1 and 5V depending on the plasma temperature (as it grows, U_a decreases). In contrast, the cathodic potential drop at a current of 50 A and higher amounts to 5-8 V. Brodskiy established the same range of cathodic voltage drop for the tungsten electrode arc. (Ref. 29). In the research of Hemmi et al. (Ref. 30), the separate estimation of the anode-fall and the cathode-fall voltages was performed for an air arc in an atmosphere burning between silver electrodes. The derived anode-fall and cathode-fall voltages proved to be about 4.5 V and 14 V, respectively. It was also found that the anode-fall and the cathode-fall voltages were almost independent of an arc current in the range from 350 to 1200 A.

Thus, the mechanism of increasing heat input into the welded metal by applying USV involves changes in the electrophysical characteristics of the discharge plasma. The analysis of the abovementioned experimental data shows that to achieve maximum heat dissipation in the anode region of the arc (during welding with a direct current of straight polarity), it is necessary to apply focused USV in the arc column and increase its power as the welding current increases.

Influence of USV on the Shape and Structure of the Arc Column

Previous studies have shown that a powerful acoustic field (up to 1.5 kW) formed by a standing wave alters the physical properties of the arc discharge (Refs. 15, 16, 19). However, the obtained results did not justify the expended energy. It can be assumed that the powerful acoustic field formed around the arc discharge dissipated most of its energy into the external environment, with only a small portion affecting the arc. Research has been conducted to investigate the influence of focused USV on the arc discharge.

The arc column without USV had a characteristic bell-shaped form (Fig. 8A). The column diameter varied from 3.0 mm (0.118 in.) near the cathode to 4.8 mm (0.189 in.) halfway along the arc and 4.4 mm (0.173 in.) at a distance of 1.0 mm (0.039 in.) from the anode. As the arc current increased from 30 to 100 A, the column diameter increases, with the increase being noticeably more intensive near the anode. Near the cathode (at a distance of 2 mm [0.078 in.]), the column diameter increased from 4.8 to 5.0 mm (0.189 to 0.197 in.), and at a distance of 1 mm from the anode, it increased from 4.4 to 4.7 mm (0.173 to 0.185 in.).

The arc column with USV was characterized by compression, and this occurred along the entire length of the arc discharge (Fig. 8B). The contraction of the arc discharge was maintained as the arc current increases. For example, at 230 A and ultrasonic power of 45 W (the maximum developed by the piezoelectric transducer), the arc diameter did not exceed 3.8 mm (0.15 in.). In contrast, without ultrasonic influence at the same operating mode, the arc diameter was 5.0–5.1 mm (0.197–0.2 in.). The maximum compression of the arc discharge occurred at a current of 150 A and full ultrasonic power, and the cross-section size of the arc was 2.9 mm (0.114 in.) (Fig. 8C).

Conclusions

This study explored the influence of focused USV in the arc column with a nonconsumable electrode on its electrophysical characteristics. The key findings of this research can be summarized as follows:

1. The influence of a focused ultrasonic field leads to an increase in the voltage of the arc discharge. The observed voltage increase at all welding modes ranged from 0.9 to 1.4 V, enhancing the arc's thermal power.

2. Focusing USV on the electrode and in the welding pool does not increase the arc voltage. However, the presence of a focused ultrasonic field in the near-electrode region of the welding arc increases its voltage by 0.9 V.

3. The potential in the cathode region increases by approximately 2 V under the influence of USV on the arc and by 0.8 V in the anode region. In contrast, the voltage in the arc column slightly decreases.

4. Under the influence of a focused ultrasonic field, there is a reduction in the arc diameter in the anode region and the column. In contrast, the diameter increases in the vicinity of the cathode region. This indicates a change in the nature of the cathode flow of charged particles in this region.

Acknowledgments

Volgograd State Technical University assisted in conducting this research under a grant from the Russian Science Foundation No. 23-13-00354, *https://rscf.ru/project/23-13-00354/*.

References

1. Razmishlyaev, A. D., Mironova, M. V., and Deli, A. A. 2008. Influence of longitudinal magnetic field on the arc characteristics at welding with the non-consumable electrode in argon. *Avtomaticheskaya Svarka* 3: 21–25.

2. Rizhov, P. N., Semenuk, V. C., and Titov, A. A. 2004. Peculiarities of joints formation and crystallization at TIG welding with arc displacement with magnetic field. *Avtomaticheskaya Svarka* 4: 17–20.

3. Boldyrev, A. M., and Birzhev, V.A. 1982. Influence of longitudinal magnetic field on the melting power of welding arc of direct polarity. *Svarochnoe Proizvodstvo* 4: 10–11.

4. Anisimov, V. V., Bukarov, V. A., and Ablamov, A. Yu. 1990. Peculiarities of non-consumable electrodes destruction under condition of magnetic field action. *Svarochnoe Proizvodstvo* 11: 38–39.

5. Zamkov, V. N., and Prilutskiy, V. P. 2004. Theory and practice of TIG-F welding (A-TIG) (Review). *Avtomaticheskaya Svarka* 9: 12–15.

6. Parshin, S. G. 2000. Composition and selection of paste fluxes for arc welding of power equipment. *Promyshlennaya Energetika* 2: 18–20.

7. Modenesi, P. J., Apolinário, E. R., and Pereira, I. M. 2000. TIG welding with single-component fluxes. *Journal of Materials Processing Technology* 99(1): 260–265. DOI: 10.1016/S0924-0136(99)00435-5

8. Tanaka, M., Shimizu, T., Terasaki, T., and Ushio, M. 2000. Effects of activating flux on arc phenomena in gas tungsten arc welding. *Science and Technology of Welding and Joining* 12: 397–402. DOI: 10.1179/136217100101538461

9. Paton, B. E., Yuschenko, K. A., and Kovalenko, D. V. 2006. Influence of the steam-gas channel on the deep penetration formation during A-TIG welding of stainless steels. *Avtomaticheskaya Svarka* 6: 3–8.

10. Zuber, M., Chaudhri, V., Suri, V. K., and Patil, S. B. 2014. Effect of flux coated gas tungsten arc welding on 304L. *International Journal of Engineering and Technology* 6(3): 177–181. DOI: 10.7763/IJET.2014.V6.691

11. Vora, J. J., and Badheka, V. J. 2016. Improved penetration with the use of oxide fluxes in activated TIG welding of low activation ferritic/martensitic steel. *Transactions of the Indian Institute of Metals* 69: 1755–1764. DOI: 10.1007/s12666-016-0835-6

12. Kazakov, Y. V., Koryagin, K. B., and Potekhin, V. P. 1989. Influence of activating fluxes on penetration at welding of steels thicker than 8 mm. *Svarochnoe Proizvodstvo* 9: 38–41.

13. Lucas, W. 2000. Activating flux - improving the performance of the TIG process. *Welding and Metal Fabrication* 68(2): 7–10.

14. Kuo, C-H., Tseng, K.-H., and Chou, C.-P. 2011. Effect of activated TIG flux on performance of dissimilar welds between mild steel and stainless steel. *Key Engineering Materials* 479: 74–80. DOI: 10.4028/www.scientific.net/KEM.479.74

15. Fan, Y. Y., Fan, C. L., Yang, C. L., Liu, W. G., and Lin, S. B. 2012. Research on short circuit transfer mode of ultrasonic assisted GMAW method. *Science and Technology of Welding and Joining* 17(3): 186–191. DOI: 10.1179/1362171811Y.0000000058

16. Wang, J., Sun, Q., Liu, Y., Wang, B., and Feng, J. 2016. Effect of pulsed ultrasonic on arc acoustic binding in pulsed ultrasonic wave-assisted pulsed gas tungsten arc welding. *Science and Technology of Welding and Joining* 23: 1362–1718. DOI: 10.1080/13621718.2016.1258812

17. Wang, J., Sun, Q., Zhang, T., Zhang, S., Liu, Y., and Feng, J. 2018. Arc characteristics in alternating magnetic field assisted narrow gap pulsed GTAW. *Journal of Materials Processing Technology* 254: 254–264. DOI: 10.1016/j.jmatprotec.2017.11.042

18. Xie, W. F., Fan, C. L., Yang, C. L., Lin, S. B., and Zhang, Y. Q. 2015. Characteristics of acoustic-controlled arc in ultrasonic wave-assisted arc. *Acta Physica Sinica* 64 (9): 412–420. DOI: 10.7498/aps.64.095201

19. Wu, C. S., Zhao, C. Y., Zhang, C., and Yongfeng, L. 2017. Ultrasonic oscillation-assisted keyholing plasma arc welding. *Welding Journal* 96: 279-s to 286-s.

20. Sun, Q. J., Lin, S. B., Yang, C. L., Fan, Y., and Zhao, G. Q. 2008. The arc characteristic of ultrasonic assisted TIG welding. *China Welding* 17(4): 52–57.

21. Xie, W. F., Fan, C. L., Yang, C. L., and Lin, S. B. 2016. Effect of acoustic field parameters on arc acoustic binding during ultrasonic wave-assisted arc welding. *Ultrasonics Sonochemistry* 29: 476–484. DOI: 10.1016/j.ultsonch.2015.11.001

22. Sun, Q. J., Lin, S. B., Yang, C. L., and Zhao, G. Q. 2009. Penetration increase of AISI 304 using ultrasonic assisted tungsten inert gas welding. *Science and Technology of Welding and Joining* 14: 765–767. DOI: 10.1179/136217109X12505932584772

23. Finkelnburg, W., and Maecker, H. 1956. Electric arcs and thermal plasma. *Handbook of Physics* 22: 254–444.

24. Leskov, G. I. 1970. *Electrical Welding Arc*. Moscow, Russia: Mashinostroenie.

25. Savinov, A. V., Lapin, I. E., and Lysak, V. I. 2011. *Arc welding with a non-melting electrode*, 477. Moscow: Mashinostroenie.

26. Lenivkin, V. A., Durgerov, N. G., and Sagirov, Kh. N. 1989. *Technological properties of the welding arc in shielding gases*, 264. Moscow: Mashinostroenie.

27. Topchiy, Yu. K., Kamenev, V. P. 1974. The device for testing the potential distribution in the arc with a non-consumable electrode. *Svarochnoe Proizvodstvo* 1: 51–22.

28. Zaruba, I. I. 1967. On the shape of the current-carrying channel of the arc column. *Avtomaticheskaya Svarka* 11: 23–26.

29. Brodskiy, A. Ya. 1956. *Argon Arc Welding with a Tungsten Electrode*. Moscow: Mashgis.

30. Hemmi, R., Yokomizu, Y., and Matsumura, T. 2003. Anode-fall and cathodefall voltages of air arc in atmosphere between silver electrodes. *Journal of Physics D: Applied Physics* 36(9): 1097–1106.

ALEXANDER SAVINOV, **ARTEM CHUDIN**, **OLEG POLESSKY** (*xxatomxx@mail.ru*), **VLADIMIR LYSAK**, **PAVEL KRASIKOV**, and **DMITRIY MURUGOV** are with Volgograd State Technical University, Volgograd, Russia.